

## Research Article

# GNSS-R Delay-Doppler Map Simulation Based on the 2004 Sumatra-Andaman Tsunami Event

**Qingyun Yan and Weimin Huang**

*Faculty of Engineering and Applied Science, Memorial University, St. John's, NL, Canada A1B 3X5*

Correspondence should be addressed to Weimin Huang; [weimin@mun.ca](mailto:weimin@mun.ca)

Received 20 March 2015; Revised 19 June 2015; Accepted 29 June 2015

Academic Editor: Jose C. Nieto-Borge

Copyright © 2016 Q. Yan and W. Huang. This is an open access article distributed under the Creative Commons Attribution License, which permits unrestricted use, distribution, and reproduction in any medium, provided the original work is properly cited.

A new method for simulating Global Navigation Satellite System-Reflectometry (GNSS-R) delay-Doppler maps (DDMs) of a tsunami-dominant sea surface is presented. In this method, the bistatic scattering Z-V model, the sea surface mean square slope model of Cox and Munk, and the tsunami-induced wind perturbation model are employed. The feasibility of the Cox and Munk model under a tsunami scenario is examined by comparing the Cox and Munk model based scattering coefficient with the Jason-1 measurement. A good consistency between these two results is obtained with a correlation coefficient of 0.93. After confirming the applicability of the Cox and Munk model for a tsunami-dominated sea, this study provides the simulations of the scattering coefficient distribution and the corresponding DDMs of a fixed region of interest before and during the tsunami. In the final analysis, by subtracting the simulation results that are free of tsunami from those with presence of tsunami, the tsunami-induced variations in scattering coefficients and DDMs can be clearly observed. As a result, the tsunami passage can be readily interpreted.

## 1. Introduction

A tsunami is a special ocean event that manifests its characteristics in terms of high propagation speed in the deep sea and extremely high wave height nearshore. It has been widely recognized that tsunamis are one of the worst natural hazards. For example, the Sumatra-Andaman tsunami that occurred in 2004 claimed many lives and caused tremendous damage to several countries [1]. Therefore, tsunami detection is especially important.

The conventional buoy measurement is a costly and inefficient method to detect tsunamis due to its high expense and low coverage [1]. The satellite altimeter may provide some direct information about the tsunami such as sea surface height (SSH) and the radar backscattering coefficient. For example, Jason-1 satellite altimeter encountered the 2004 Sumatra-Andaman tsunami on its path 109 for cycle 129, thereby offering valuable data on tsunami measurement [2]. However, only a handful of definitive SSH changes due to a tsunami event have been measured out of more than 150 documented tsunami events since the launch of the TOPEX/Poseidon satellite altimeter in 1992 [3]. This is mainly

because of the limited coverage of the satellite altimeter [2]. Recently, GNSS-R emerged as an efficient and accurate technique for ocean remote sensing due to its advantages in temporal and spatial coverage and immunity to weather effects [4]. Those benefits of the application of GNSS-R may provide a promising solution to tsunami remote sensing. Moreover, manifestations of a tsunami in the deep ocean have been investigated by a large amount of researchers, thereby laying a theoretical foundation for the GNSS-R-based deep sea tsunami detection. In 1996, tsunami-induced variations in sea surface roughness were first reported by Walker [5] and were given the name “tsunami shadow” based on observations of the darkened stripes along the tsunami front. Later, Godin [6] explained that the tsunami-induced changes in sea surface roughness are due to the tsunami-induced perturbations in sea surface wind speed. Based on these results, a theoretical model for the calculation of tsunami-induced sea surface wind velocity has been developed in [2].

In addition, recent research has made significant development on GNSS-R DDM-based sea surface wind remote sensing (e.g., [7–9]). These works have also contributed to the DDM simulation in this paper for a tsunami-dominated

sea surface, which is based upon the tsunami-perturbed sea surface wind speed. There are a few reports (e.g., [1, 10, 11]) in the literature about the GNSS-R altimetry-based tsunami detection. However, there is no publication on tsunami detection from GNSS-R DDM, to the authors' knowledge. In this paper, a process for simulating tsunami-dominant sea surface DDM is proposed. This method is based on the Zavorotny and Voronovich (Z-V) bistatic scattering model [12], the Cox and Munk sea surface mean square slope model [13], and the tsunami-induced wind speed perturbation model [2]. Followed by the introduction to this method, the feasibility of the Cox and Munk model [13] under a tsunami scenario is examined by comparing the simulated scattering coefficient with the Jason-1 measurement. After verifying its applicability, the tsunami DDM simulation can be achieved through inputting the background wind speed over the sea surface and the tsunami-induced sea surface change. In this work, the simulation results before and during a tsunami over a region of interest are presented. Through analysis, the passage of the tsunami over this region can be interpreted based on the observation of tsunami-induced variations in scattering coefficient and DDMs. This work may provide some new support for the GNSS-R DDM-based tsunami detection in the future.

The remainder of this paper is organized as follows. The procedures of tsunami-dominant sea surface DDM simulation are described in Section 2. The verification of the Cox and Munk model under a tsunami scenario followed by the simulation results is presented in Section 3. Conclusions are presented in Section 4.

## 2. Model Implementation and Simulation Process

The Cox and Munk model [13] and the Z-V model [12] have already been successfully applied to the GNSS-R DDM-based sea surface wind sensing (e.g., [7, 14]). The Z-V model depicts the scattered GPS signal power as a function of time delay and Doppler frequency shift, the transmitter elevation angle, and the receiver height as well as the surface scattering coefficient ( $\sigma^0$ ). The Cox and Munk model substantiates an empirical relationship between the wind speed at the height of 10 m above the sea surface ( $U_{10}$ ) and the sea surface mean square slope (MSS). Consequently, the sea surface scattering coefficient is determined by MSS [7]. In summary, with knowledge of  $U_{10}$  the corresponding DDM can be simulated by combining the Cox and Munk model and the Z-V model. With this in mind, the associated DDM simulation can be completed if the distribution of  $U_{10}$  over a tsunami-dominant sea surface is available.

The Z-V model [12] can be described as follows:

$$\begin{aligned} & \langle |Y(\tau, f_D)|^2 \rangle \\ &= T_i^2 \iint_A \frac{D^2(\vec{\rho}) \sigma^0(\vec{\rho}) \Lambda^2(\tau) |S(f_D)|^2}{4\pi R_R^2(\vec{\rho}) R_T^2(\vec{\rho})} d^2\rho, \end{aligned} \quad (1)$$

where  $\tau$  is the time delay between the received signal and the local code replica,  $\Lambda(\tau) = 1 - |\tau/\tau_c|$ , when  $-\tau_c \leq \tau \leq \tau_c$ ;

$\Lambda = 0$ ; otherwise  $\tau_c$  is the length of one code chip. Consider  $S(f_D) = \sin(\pi T_i f_D)/(\pi T_i f_D)$ ,  $T_i$  is the coherent integration time,  $\vec{\rho}$  is the displacement vector of a surface point from the specular point (SP),  $D$  is the antenna radiation pattern,  $R_T$  and  $R_R$  are the distances from a point on the ocean surface to the GNSS-R transmitter and receiver,  $A$  represents the effective scattering surface area (glistening zone), and  $\sigma^0$  is the surface scattering coefficient.

With the exception of  $\sigma^0$ , the rest of the terms in (1) are usually known for a specific GNSS system and its geometry. Therefore, we mainly consider the scattering coefficient  $\sigma^0$ , which may be written as [7]

$$\sigma^0(\vec{\rho}) = \pi |\mathfrak{R}|^2 P\left(-\frac{q_\perp}{q_z}\right) \left(\frac{q}{q_z}\right)^4, \quad (2)$$

where  $|\mathfrak{R}|^2$  is the Fresnel reflection coefficient that depends on the local elevation angle, polarization, and the complex dielectric constant of sea water [7]; the scattering vector  $\vec{q}$  can be obtained with the locations of the transmitter, receiver, and corresponding surface point;  $-q_\perp/q_z$  is the ocean surface slope, denoted hereafter as  $s$ .  $P(s)$  is the slope Probability Density Function (PDF) of the ocean surface gravity wave which is believed to be subject to Gaussian distribution with wind-dependent upwind variance  $\sigma_u^2$  and crosswind variance  $\sigma_c^2$  [15]. It is worth mentioning that tsunami waves are gravity waves.  $P(s)$  is expressed as [7]

$$\begin{aligned} P(s) &= \frac{1}{2\pi \sqrt{\det(W)}} \exp\left[-\frac{1}{2} \begin{pmatrix} s_x \\ s_y \end{pmatrix}^T W^{-1} \begin{pmatrix} s_x \\ s_y \end{pmatrix}\right], \\ W &= \begin{bmatrix} \cos \phi_0 & -\sin \phi_0 \\ \sin \phi_0 & \cos \phi_0 \end{bmatrix} \times \begin{bmatrix} \sigma_u^2 & 0 \\ 0 & \sigma_c^2 \end{bmatrix} \\ &\times \begin{bmatrix} \cos \phi_0 & \sin \phi_0 \\ -\sin \phi_0 & \cos \phi_0 \end{bmatrix}, \end{aligned} \quad (3)$$

where  $\phi_0$  is the angle between the up-down wind direction and the  $x$ -axis. Subsequently, the clean sea surface mean square slope model of Cox and Munk [13] is introduced to link the wind speed and wind direction to the upwind and crosswind variances, as

$$\begin{aligned} \sigma_u^2 &= 0.45 \times (3.16 \times 10^{-3} f(U_{10})), \\ \sigma_c^2 &= 0.45 \times (0.003 + 1.92 \times 10^{-3} U_{10}), \end{aligned} \quad (4)$$

where

$$f(U_{10}) = \begin{cases} U_{10} & U_{10} \leq 3.49 \\ 6 \cdot \ln(U_{10}) - 4 & 3.49 < U_{10} \leq 46 \\ 0.411 \cdot U_{10} & U_{10} > 46. \end{cases} \quad (5)$$

Following similar steps as presented in [7, 14], the DDMs can be readily simulated with the knowledge of  $U_{10}$ , based on the Cox and Munk model [13] and the Z-V model [12] for a tsunami-free sea surface.

For a tsunami-dominant sea surface, the effective wind speed can be derived from the tsunami-induced wind speed perturbation model [2], that is, the so-called Godin model. This model was proposed based on the observation data of “tsunami shadow” from the October 4, 1994, Hokkaido tsunami [5]. The theoretical derivation of this model and its validation based on simulation were presented in [2]. Moreover, this model has been successfully applied in the simulation of radar backscattering strength over a tsunami region (e.g., [2, 3]). The tsunami-induced variations in radar backscattering strength estimated based on the Godin model were consistent with the Jason-1 measurement [2]. Thus, the Godin model is employed here to determine the effective wind speed during a tsunami period. This model shows that the effective wind speed during a tsunami event depends on tsunami parameters and differs from the background wind speed by a factor of  $M$  [2], and

$$M = 1 - \frac{\kappa ac}{Hu_* \ln \beta}, \quad (6)$$

where  $\kappa = 0.4$ ,  $u_* = 0.04U_{10}$ ,  $H$  is the height of the background logarithmic boundary layer,  $a$  is the sea surface height change due to tsunami,  $c = \sqrt{gD}$  is the tsunami phase speed, where  $g$  is the acceleration due to gravity,  $D$  is the depth of sea, and

$$\beta = \frac{\kappa u_* T_0}{2\pi z_0}, \quad (7)$$

where  $z_0 = 0.01u_*^2/g$  represents the roughness length and  $T_0$  is tsunami period.

By employing these models, the tsunami DDMs can be simulated with different tsunami parameters and background wind speed.

### 3. Simulation Results

In this section, feasibility of the Cox and Munk model under a tsunami scenario is tested first. Then, the parameters associated with tsunami DDM simulation are set. After that, the tsunami DDM simulation results are presented.

**3.1. Feasibility of the Cox and Munk Model under a Tsunami Scenario.** The Jason-1 satellite altimeter encountered the tsunami on the morning of December 26, 2004 [2] (shown in Figure 1). It recorded radar backscattering coefficient and sea surface wind speed, thereby offering an opportunity to study the wind speed and  $\sigma^0$  during the tsunami event. Before exerting the tsunami DDM simulation, the feasibility of the Cox and Munk model under a tsunami event should be examined. By employing the Cox and Munk model, the  $\sigma^0$  of a tsunami-dominant sea surface can be simulated with the knowledge of  $U_{10}$  over the corresponding region. Based on this, a comparison between the Jason-1 measured  $\sigma^0$  and the simulated  $\sigma^0$  can be made.

Figure 2(a) illustrates the Jason-1 measured sea surface wind speeds (solid line) over the range of (6.00°S, 83.60°E) to (4.99°N, 87.54°E) with the presence of the tsunami leading

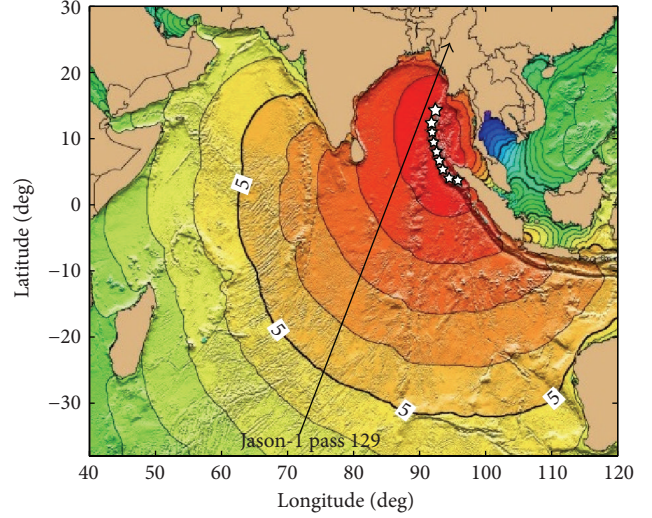


FIGURE 1: Jason-1 satellite altimeter ground track during the 2004 Sumatra-Andaman tsunami. Black line indicates the Jason-1 ground track with a direction in accordance with the arrow. White stars represent the epicentre. Contours of the tsunami leading front are also shown with hourly intervals. This graphic is modified from the work of the National Geophysical Data Center/NOAA, at [http://www.ngdc.noaa.gov/hazard/img/2004\\_1226.jpg](http://www.ngdc.noaa.gov/hazard/img/2004_1226.jpg).

wave front. For the simulation, some assumptions are made below:

- (1) The GNSS-R transmitter, receiver, and the SP are set on the same line that is also perpendicular to the sea surface.
- (2) The SP follows the Jason-1 ground track.
- (3) The Jason-1 measured  $U_{10}$  is uniform along tsunami wave front.

The first assumption is required to simulate the Jason-1 backscattering scenario. The second assumes that the GNSS-R system and Jason-1 monitored this region at the same time. The last one aims at forming a two-dimensional wind speed distribution over the glistening zone.

The size of GNSS-R glistening zone is about 200 km by 200 km. Through inputting the wind speeds that are interpolated using the Jason-1 measured  $U_{10}$  over sea surface, the scattering coefficient can therefore be simulated. Here, only the  $\sigma^0$  at SP which follows the Jason-1 ground track is recorded and compared with the Jason-1 measurements. Figure 2(b) shows the  $\sigma^0$  measured by Jason-1 and the  $\sigma^0$  simulated by the Cox and Munk model. A good consistency between the measured  $\sigma^0$  and the simulated  $\sigma^0$  can be observed with a correlation coefficient of 0.93. In Figure 2(b), the simulated scattering coefficients for GNSS-R seem to be slightly overestimated compared to the measurement by Jason-1. This is mainly due to the difference in the operating frequencies of GNSS-R (1.5 GHz, i.e., L-band) and Jason-1 (5.4 GHz, i.e., C-band). The average difference of the scattering coefficient is about 1.33 dB and this is consistent with the analysis in [16], where the difference of  $\sigma^0$  between

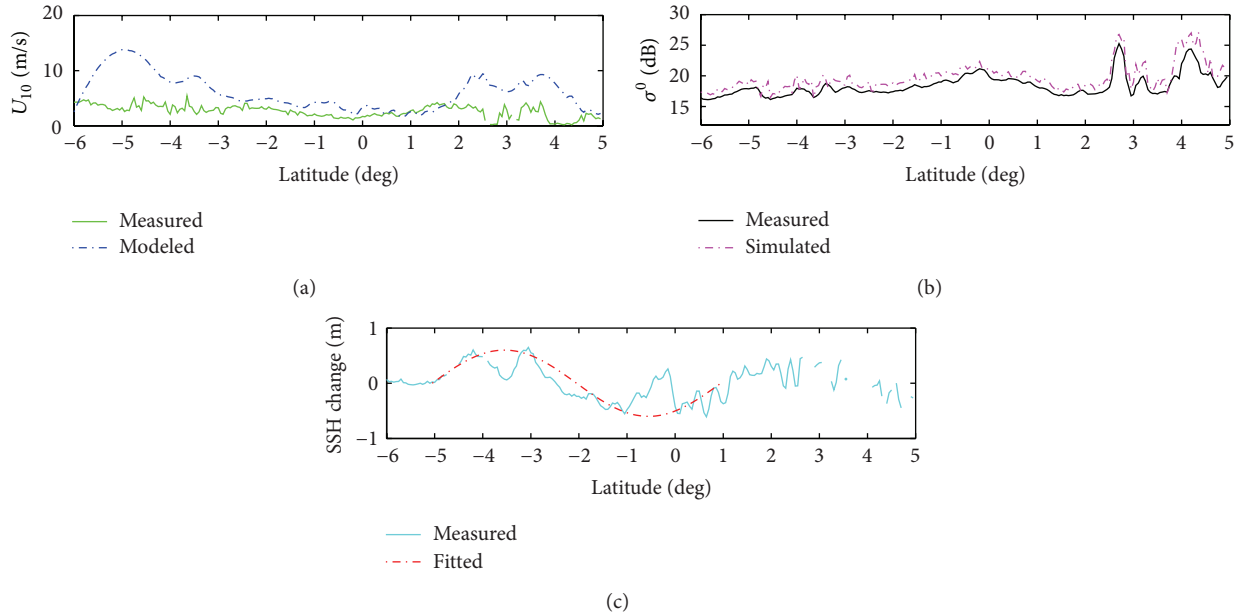


FIGURE 2: Jason-1 measurement for pass 129 from (6.00°S, 83.60°E) to (4.99°N, 87.54°E) obtained during the 2004 tsunami: (a) sea surface  $U_{10}$ , (b) backscattering coefficient  $\sigma^0$ , and (c) SSH change due to a tsunami. Gaps in the curves are caused by deficiency of measured data.

L- and C-band measurements is found to be about 2 dB. Therefore, the feasibility of the Cox and Munk model on the tsunami DDM simulation is confirmed.

**3.2. Simulation Scenario Parameters.** Based on the analysis above, it can be concluded that the  $\sigma^0$  of a tsunami-dominant sea surface can be simulated via the Cox and Munk model [13]. Thus, the tsunami DDMs can be simulated through the Z-V model [12], the Cox and Munk model [13], and the tsunami-induced wind speed perturbation model [2] with reliability.

Here, to facilitate the simulation, the typical empirical values are adopted in alignment with those in [2]; that is,  $T_0 = 40$  min,  $D = 4000$  m, and  $H = 60$  m. If the SSH change  $a$  due to tsunami and the background wind speed are known, the effective wind speed over a tsunami surface can therefore be determined by implementing the tsunami-induced wind speed perturbation model [2].

The SSH measured by Jason-1 on cycle 109 during the tsunami event is subtracted by the average SSH observed over the exactly same ground track on cycles 108 and 110, and the difference is regarded as tsunami-induced SSH change  $a$  (shown in Figure 2(c)). This process is in accord with [17]. Besides, it has been reported in [17] that the tsunami-induced SSH change  $a$  over the range from (5.00°S, 83.96°E) to (1.00°N, 86.12°E) can be well fitted by a sine wave with a wavelength of 580 km and an amplitude of 60 cm, as shown by a dash line in Figure 2(c). Alternatively, the sine model is treated as another form of input  $a$  for reference. In addition,  $a$  is assumed to distribute uniformly along the contours of the tsunami leading wave front, which are concentric circles with a center at the epicenter (3.4°N, 94.2°E).

The  $U_{10}$  over the region under investigation measured by QuikSCAT on its orbit 28744 is considered to be the

background wind speed. The data was recorded around 45 min before the earthquake appeared, which means this measurement is totally free of the tsunami influence. Therefore, it is reasonable to use the QuikSCAT measurement as the background  $U_{10}$ . The effective  $U_{10}$  is calculated using only the QuikSCAT measurement over the Jason-1 ground track and is shown in Figure 2(a). Difference between the modelled and measured wind speeds can be seen in Figure 2(a). This is because the modelled wind speed significantly relies on the background wind speed (i.e., before the appearance of tsunami). The only available background wind speed data of the region under investigation, immediately before the tsunami, was measured by QuikSCAT. However, the data was collected 45 min before the earthquake happened. Moreover, Jason-1 flew over the same region 115 min after the earthquake appeared. Thus, a time gap of 160 min exists between the measured and the modelled wind speeds. As we know, wind speed may change significantly after two hours. This may explain the difference between the modelled and measured wind speeds.

The parameters mentioned above are tabulated in Table 1. In terms of GNSS-R simulation scenario, the parameters are kept the same as those in [18], also shown in Table 1.

In order to manifest a unique influence of the tsunami on GNSS-R sea surface remote sensing in this work, a continuous detection over a fixed region is assumed. To achieve this, both the transmitter and the receiver are set fixed over time. In this fashion, the variations caused by the geometry change of GNSS-R system will be eliminated as well, which allows a more direct observation of tsunami effect. The region of our interest is set around (6.0081°S, 83.6019°E) with a size of 200 km by 200 km. The first simulation result was conducted for 02:55:22 UT. The study region at this time was tsunami-free. Therefore, this first simulation result is considered as

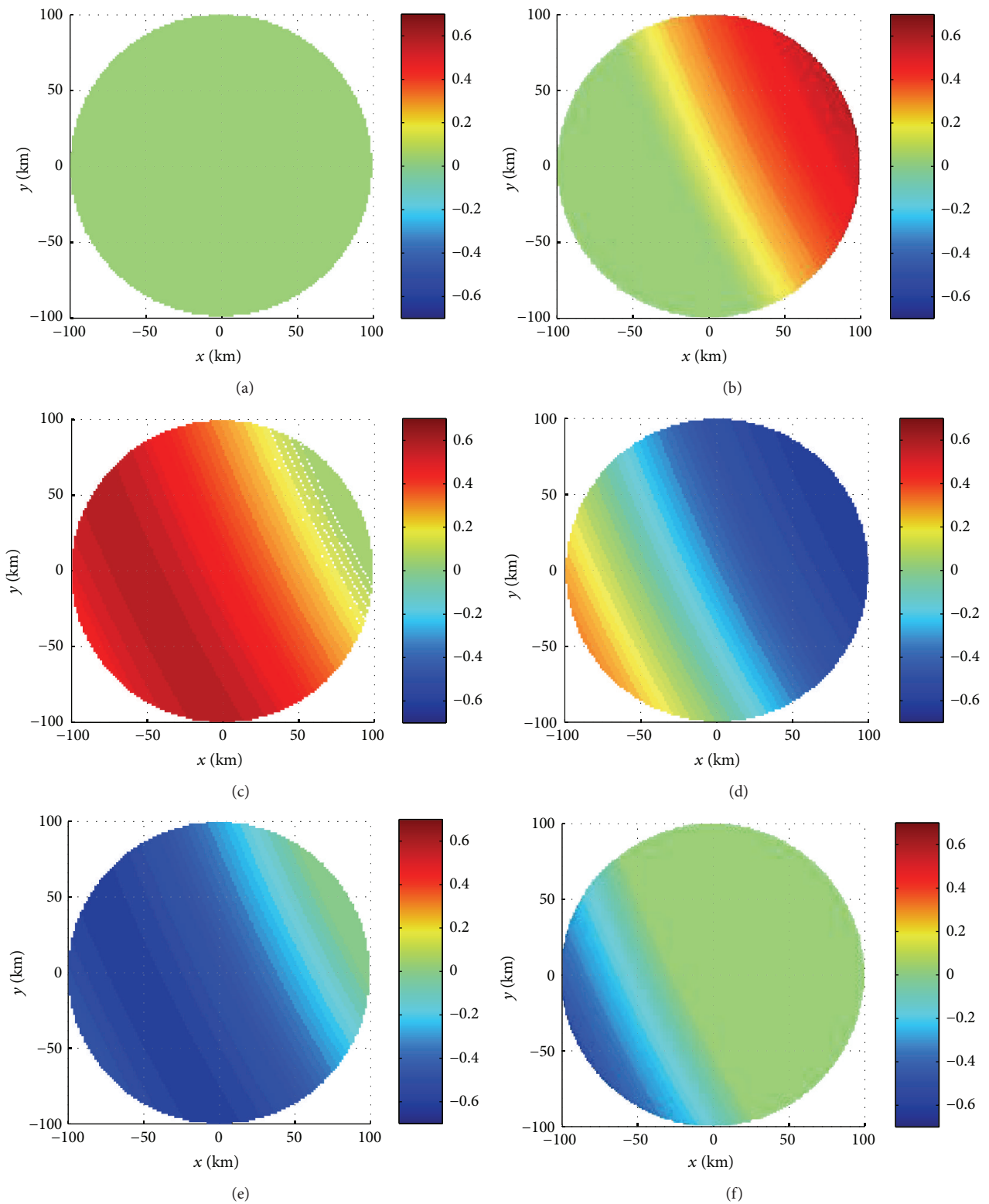


FIGURE 3: Spatial distribution of tsunami-induced SSH change based on a sine wave model: (a) before tsunami and with (b) a part of tsunami leading front, (c) the tsunami crest, (d) a part between the crest and trough, (e) the tsunami trough, and (f) the tail of tsunami leading front.

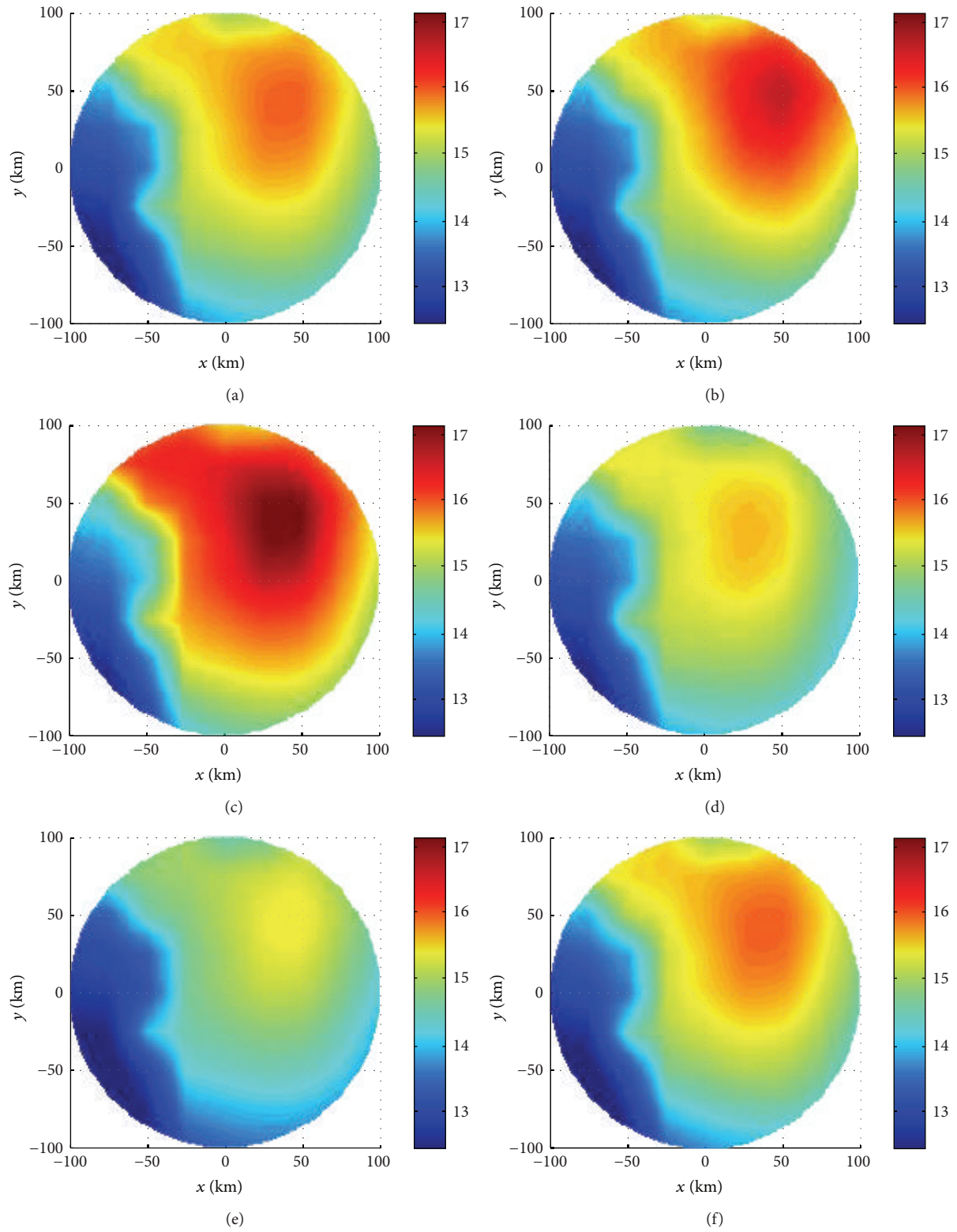


FIGURE 4: Simulated  $\sigma^0$  using fitted sine wave as input: (a) without tsunami and with (b) a part of tsunami leading front; (c) the tsunami crest; (d) a part between the crest and trough; (e) the tsunami trough; and (f) the tail of tsunami leading front.

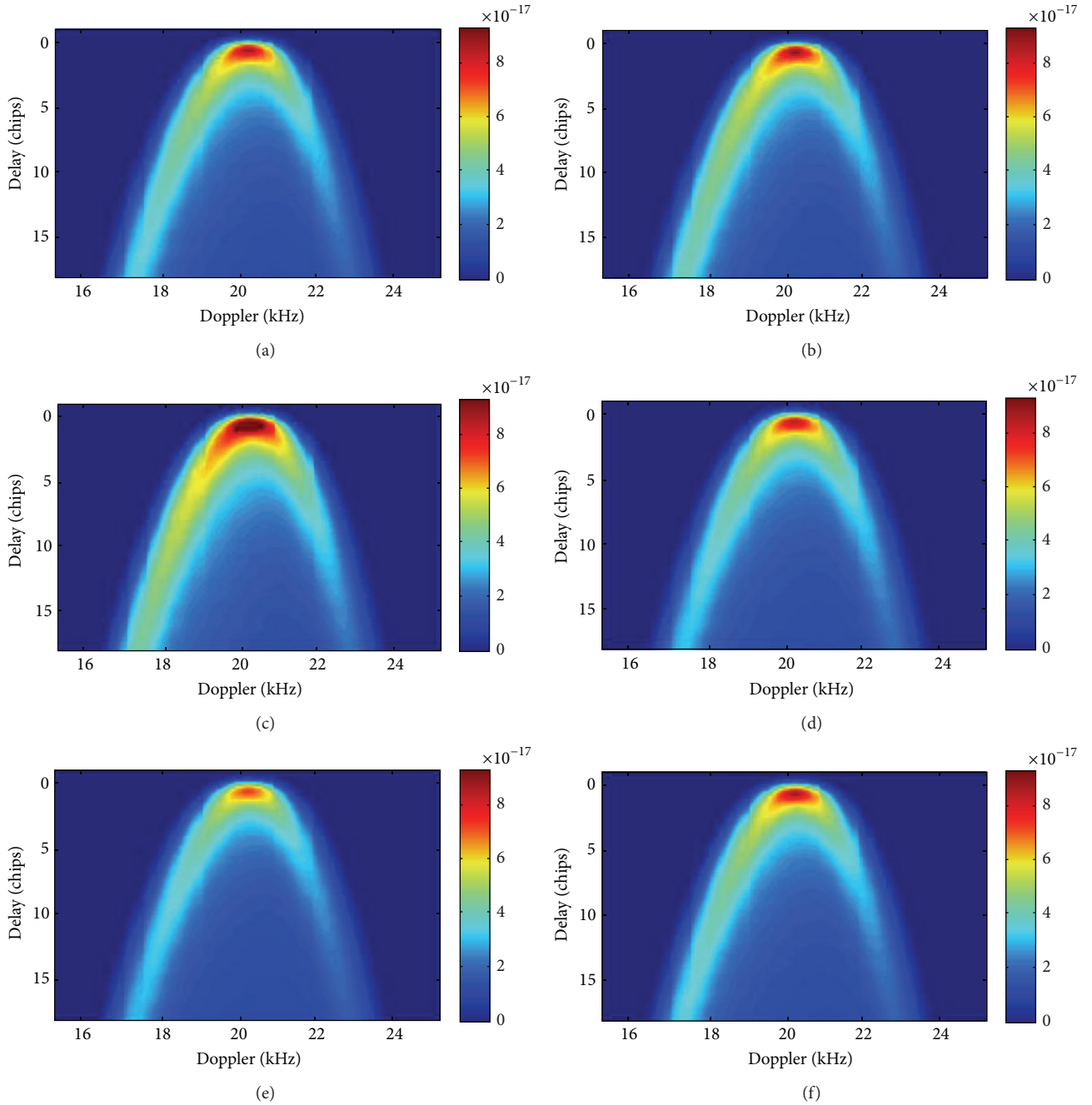


FIGURE 5: Corresponding DDMs resulting from  $\sigma^0$  in Figure 4.

the initial baseline for the following results. Meanwhile, the SSH change in Figure 2(c) is regarded as initial distribution. The initial simulation only depends on the background  $U_{10}$  over this region measured by QuikSCAT. However, within a few minutes, this region experienced a tsunami passage. The tsunami-induced wind speed perturbation model must be employed with the tsunami entering into this region. The effective  $U_{10}$  will be calculated based on this model with the knowledge of background  $U_{10}$  and  $a$ .

As we have assumed  $D = 4000$  m, the tsunami propagation speed can thus be approximated by 200 m/s. Meanwhile,

the initial distribution of  $a$  over space is known. For this reason, the  $a$  over this region at each moment can be easily deduced according to the distance and tsunami propagation speed. Then, the effective  $U_{10}$  at different time can also be determined.

**3.3. Results.** The spatial distribution of tsunami-induced SSH change based on a sine wave model is shown in Figure 3.

Figure 4 displays the simulated  $\sigma^0$  by adopting the fitted sine wave model as input  $a$ . The time gaps between the initial detection in Figure 4(a) and those from Figures

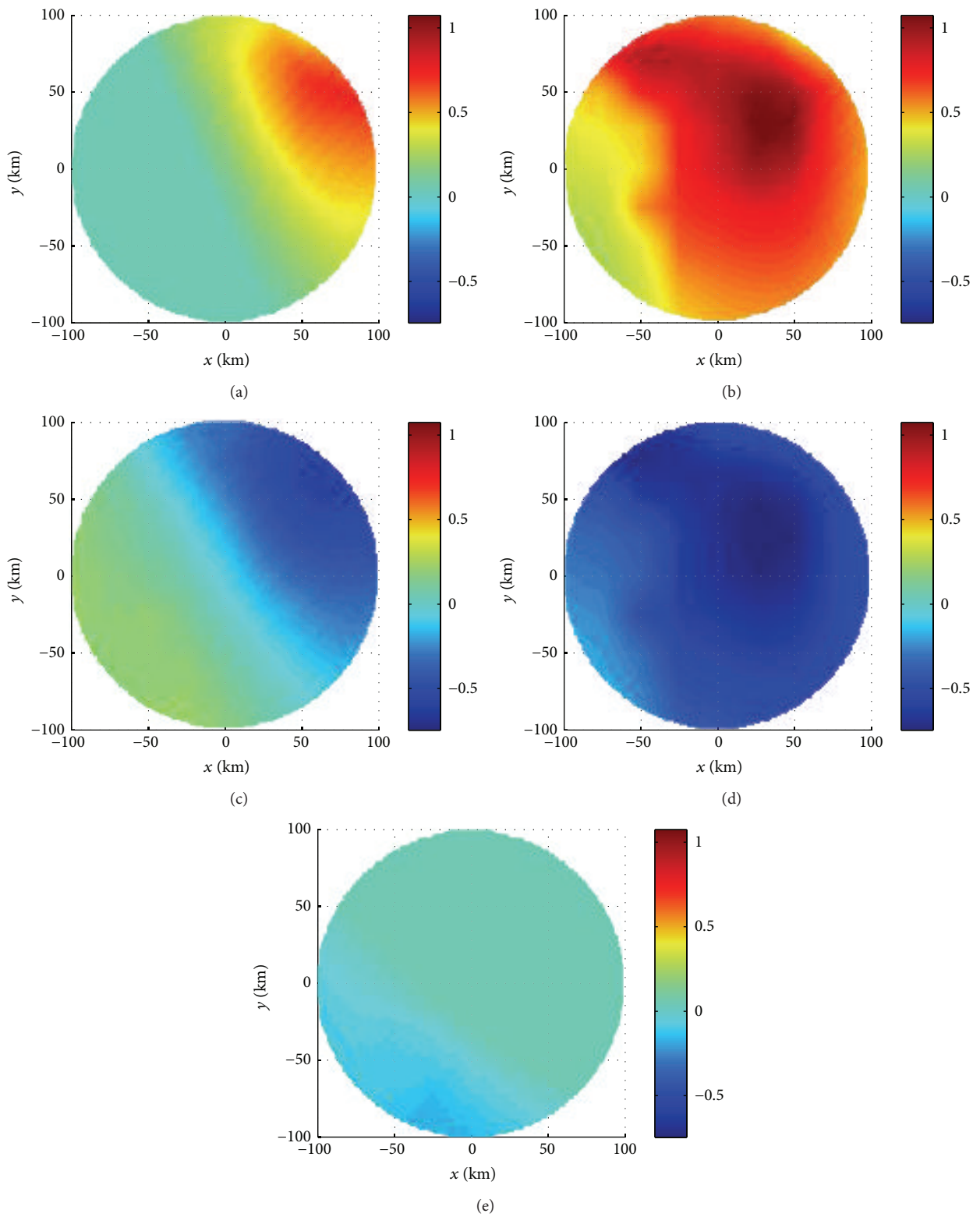


FIGURE 6: Differences of the scattering coefficients of tsunami-dominated and tsunami-free sea surfaces (based on sine wave-modelled SSH changes).

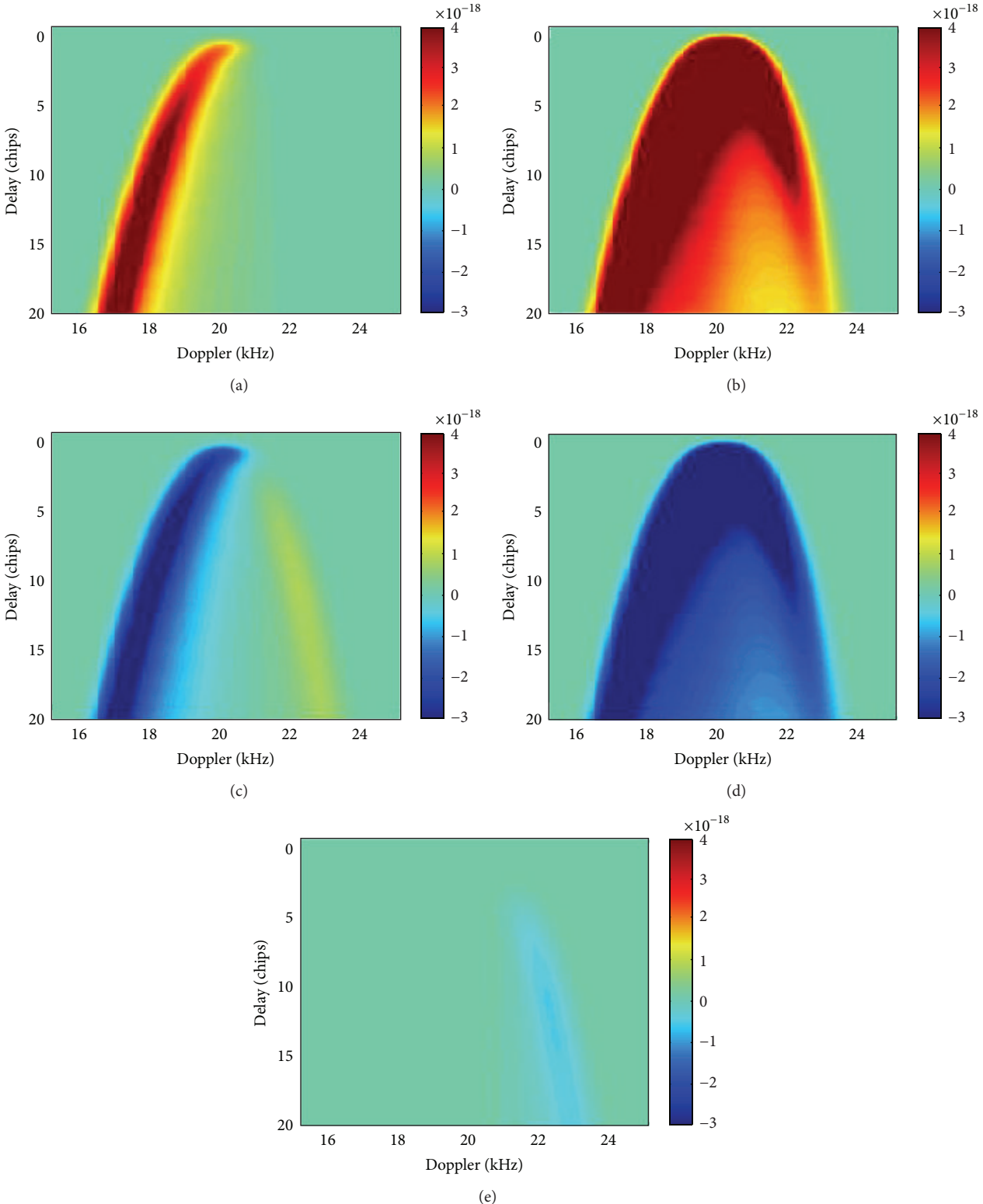


FIGURE 7: Differences of the DDMs of tsunami-dominated and tsunami-free sea surfaces (based on sine wave-modelled SSH changes).

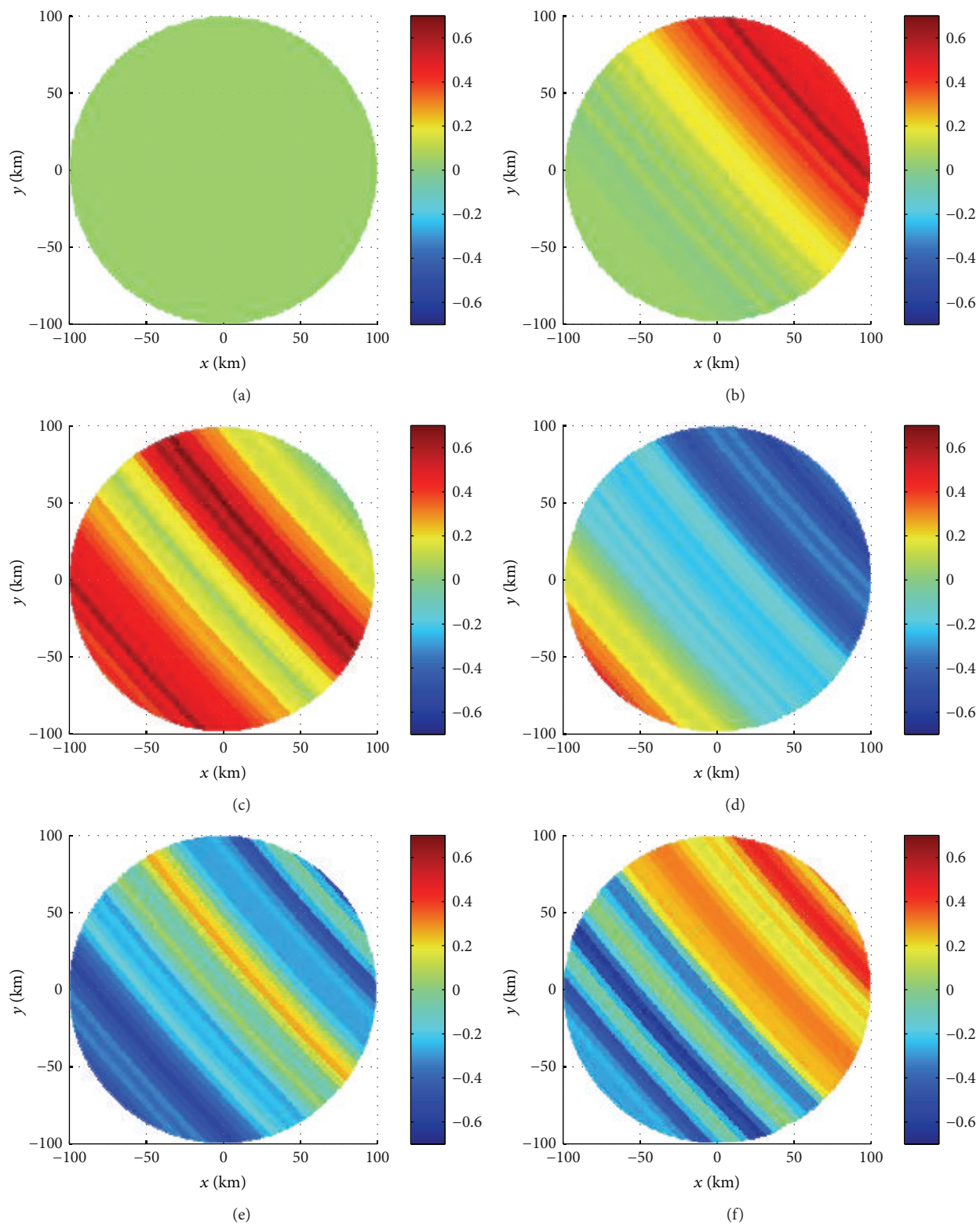


FIGURE 8: Spatial distribution of tsunami-induced SSH change based on Jason-1 measurements.

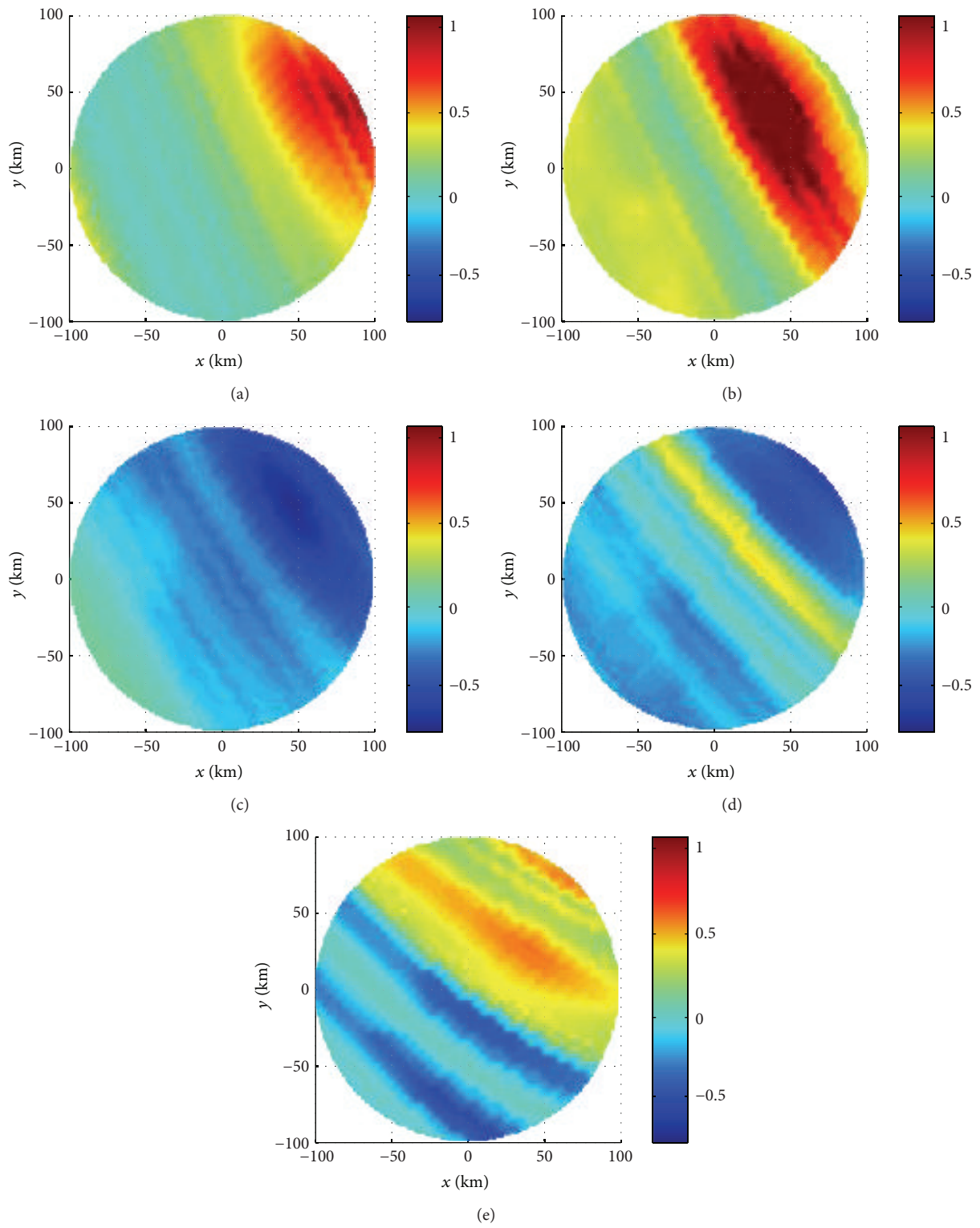


FIGURE 9: Differences of the scattering coefficients of tsunami-dominated and tsunami-free sea surfaces (based on Jason-1 measured SSH changes).

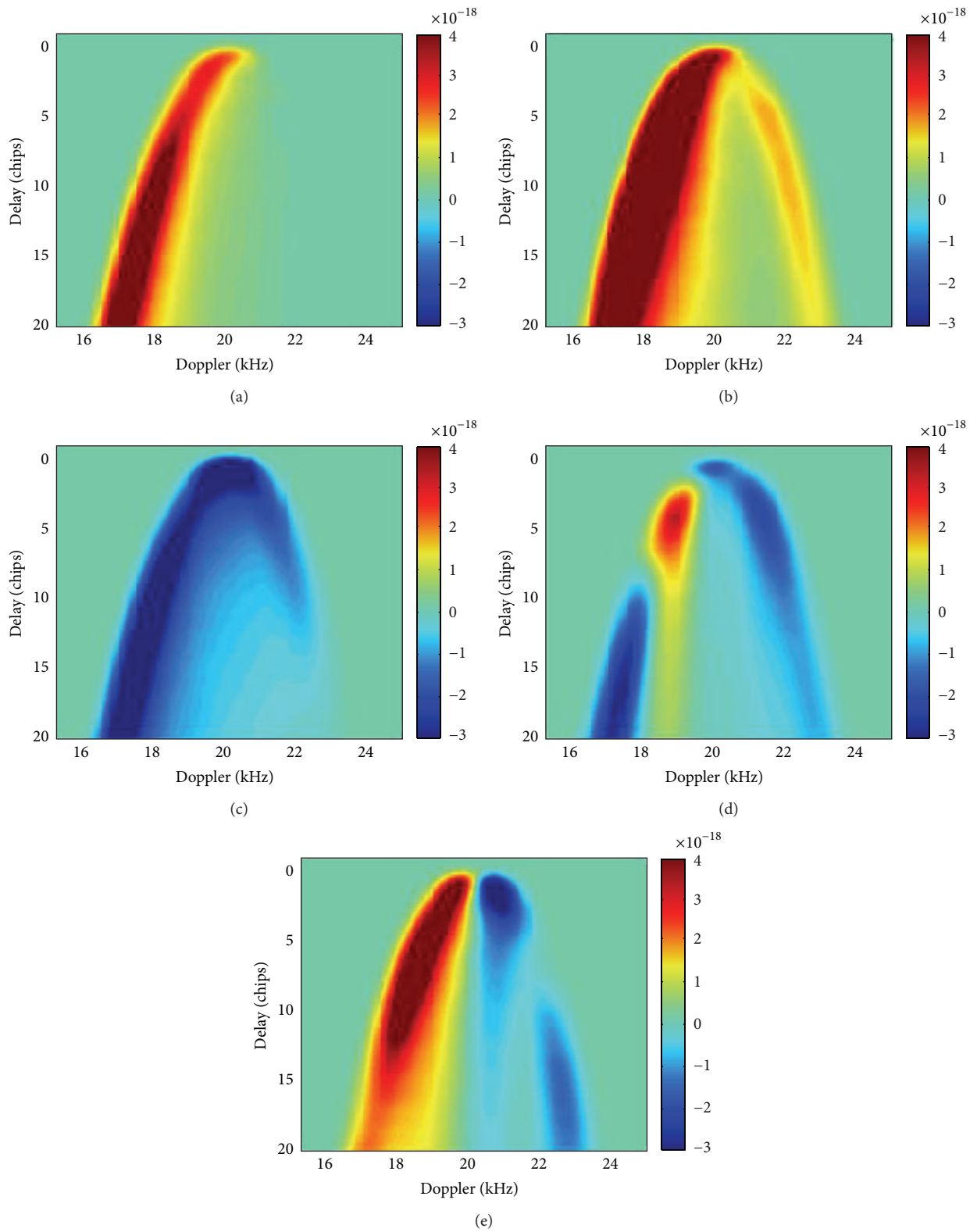


FIGURE 10: Differences of the DDMs of tsunami-dominated and tsunami-free sea surfaces (based on Jason-1 measured SSH changes).

TABLE 1: Tsunami DDM simulation setting up.

Simulation parameters	Value (data source)
Tsunami period ( $T_0$ )	40 min
Depth of ocean ( $D$ )	4000 m
Height of the background logarithmic boundary layer ( $H$ )	60 m
SSH change ( $a$ )	Jason-1 measurement/fitted sine wave model
Background wind speed	QuikSCAT measurement on orbit 28744
Receiver height	680 km
Transmitter velocity	(-2.72, 2.68, -.65) km/s
Receiver velocity	(7.21, 1.23, 1.72) km/s
SP position	(6.0081°S, 83.6019°E)

4(b) to 4(f) are 9.17 min, 22.92 min, 36.67 min, 50.42 min, and 64.17 min, respectively. Figure 5 shows the simulated DDMs corresponding to the scattering coefficient maps in Figure 4. In order to manifest the tsunami-induced variations in  $\sigma^0$  and DDMs, the simulation results with tsunami are subtracted by the initial result that contains no tsunami; that is, subplots (b)–(f) in both Figures 4 and 5 are subtracted by the corresponding subplot (a). The resultant scattering coefficient and DDM differences are displayed in Figures 6 and 7, respectively. Although the overall shapes in each subplot of Figure 4 or Figure 5 are similar, variations still can be observed. From Figure 6, the  $\sigma^0$  variations caused by the tsunami are found to be about  $\pm 1$  dB. This result is consistent with the analysis in [2].

Intuitively, an increase in  $a$  will lead to a reduction in  $M$  factor according to (6). On the other hand, a decrease in  $U_{10}$  will contribute to an increase in  $\sigma^0$ . On the whole, the variations in  $\sigma^0$  are coincident with the changes of  $a$ . Therefore, the passage of the tsunami can be identified from Figure 6: (a) the leading front appears first; (b) then comes the crest; (c) the transition region between the crest and the trough approaches later; (d) after that, the trough emerges; and (e) finally, the tsunami wave propagates out of this region with only a small portion of the tail remaining. The variations in  $\sigma^0$  are approximately proportional to the tsunami-induced SSH changes. The tsunami-induced variations in DDMs can be observed in Figure 7.

The spatial distribution of tsunami-induced SSH change based on Jason-1 measurements is shown in Figure 8. Since the variations due to tsunami are not so obvious in simulated scattering coefficient maps and DDMs, only the differences between the results with and without tsunami are displayed in Figures 9–10. Due to the non-ideal-sine distribution of measured  $a$ , these simulation results differ slightly from those based on fitted sine wave input  $a$ . However, with a close observation of Figure 9, the variations in  $\sigma^0$  are also consistent with the distribution of measured  $a$ .

#### 4. Conclusion

In this work, a process is proposed to simulate the DDM of a tsunami-dominant sea surface. The Z-V model, the

Cox and Munk model, and the tsunami-induced wind speed perturbation model are employed in this method. The feasibility of Cox and Munk model under the tsunami scenario is confirmed (a correlation coefficient of 0.93 between the simulated and measured  $\sigma^0$  is observed). After verifying the applicability of the Cox and Munk model for a tsunami-dominated sea,  $\sigma^0$  and DDMs are simulated with two different tsunami-induced SSH change inputs, that is, Jason-1 measurement and fitted sine wave model. The  $\sigma^0$  variations caused by the tsunami are found to be about  $\pm 1$  dB, which is consistent with the result in [2]. Finally, by studying the tsunami-induced variations in  $\sigma^0$ , the passage of tsunami can be identified. In the future, tsunami parameters may be retrieved from the simulated DDMs of tsunami-dominant sea surface. It is also necessary to further validate the proposed method using collected GNSS-R data and corresponding measured background and effective wind speed dataset during a tsunami event. However, this study is not possible today as the available data for this research is limited. This may become possible with the launch of new spaceborne GNSS-R missions, for example, TechDemoSat-1 and Cyclone GNSS (CYGNSS) [19].

#### Conflict of Interests

The authors declare that there is no conflict of interests regarding the publication of this paper.

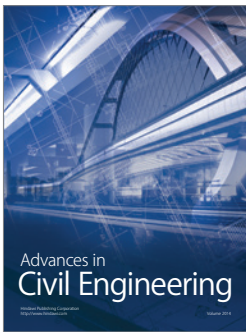
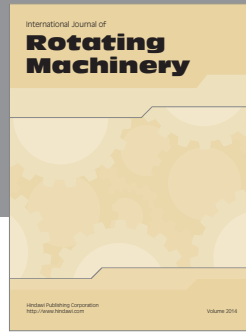
#### Acknowledgments

This work was supported by the Natural Sciences and Engineering Research Council of Canada Discovery Grant (NSERC 402313-2012) to Dr. Weimin Huang. The authors would like to thank C. Arbour for her editorial help on this paper.

#### References

- [1] K. Yu, "Tsunami-wave parameter estimation using GNSS-based sea surface height measurement," *IEEE Transactions on Geoscience and Remote Sensing*, vol. 53, no. 5, pp. 2603–2611, 2015.
- [2] O. A. Godin, V. G. Irisov, R. R. Leben, B. D. Hamlington, and G. A. Wick, "Variations in sea surface roughness induced by the 2004 Sumatra-Andaman tsunami," *Natural Hazards and Earth System Science*, vol. 9, no. 4, pp. 1135–1147, 2009.
- [3] B. D. Hamlington, R. R. Leben, O. A. Godin, and V. G. Irisov, "On the feasibility of tsunami detection using satellite-based sea surface roughness measurements," in *Proceedings of the 30th IEEE International Geoscience and Remote Sensing Symposium (IGARSS '10)*, pp. 3035–3038, Honolulu, Hawaii, USA, July 2010.
- [4] S. Jin, G. P. Feng, and S. Gleason, "Remote sensing using GNSS signals: current status and future directions," *Advances in Space Research*, vol. 47, no. 10, pp. 1645–1653, 2011.
- [5] D. A. Walker, "Observations of tsunami 'shadows': a new technique for assessing tsunami wave heights?" *Science of Tsunami Hazards*, no. 14, pp. 3–11, 1996.
- [6] O. A. Godin, "Air-sea interaction and feasibility of tsunami detection in the open ocean," *Journal of Geophysical Research C: Oceans*, vol. 109, no. 5, Article ID C05002, pp. 1–20, 2004.

- [7] C. Li and W. Huang, "An algorithm for sea-surface wind field retrieval from GNSS-R delay-doppler map," *IEEE Geoscience and Remote Sensing Letters*, vol. 11, no. 12, pp. 2110–2114, 2014.
- [8] N. Rodriguez-Alvarez, D. M. Akos, V. U. Zavorotny, J. A. Smith, A. Camps, and C. W. Fairall, "Airborne GNSS-R wind retrievals using delay-doppler maps," *IEEE Transactions on Geoscience and Remote Sensing*, vol. 51, no. 1, pp. 626–641, 2013.
- [9] E. Valencia, V. U. Zavorotny, D. M. Akos, and A. Camps, "Using DDM asymmetry metrics for wind direction retrieval from GPS ocean-scattered signals in airborne experiments," *IEEE Transactions on Geoscience and Remote Sensing*, vol. 52, no. 7, pp. 3924–3936, 2014.
- [10] M. Martin-Neira, C. Buck, S. Gleason et al., "Tsunami detection using the PARIS concept," in *Proceedings of the Progress in Electromagnetics Research Symposium*, Hangzhou, China, August 2005.
- [11] R. Stosius, G. Beyerle, A. Hoehner, J. Wickert, and J. Lauterjung, "The impact on tsunami detection from space using GNSS-reflectometry when combining GPS with GLONASS and Galileo," *Advances in Space Research*, vol. 47, no. 5, pp. 843–853, 2011.
- [12] V. U. Zavorotny and A. G. Voronovich, "Scattering of GPS signals from the ocean with wind remote sensing application," *IEEE Transactions on Geoscience and Remote Sensing*, vol. 38, no. 2, pp. 951–964, 2000.
- [13] C. Cox and W. Munk, "Measurement of the roughness of the sea surface from photographs of the sun's glitter," *Journal of the Optical Society of America*, vol. 44, no. 11, pp. 838–850, 1954.
- [14] M. P. Clarizia, C. P. Gommenginger, S. T. Gleason, M. A. Srokosz, C. Galdi, and M. Di Bisceglie, "Analysis of GNSS-R delay-Doppler maps from the UK-DMC satellite over the ocean," *Geophysical Research Letters*, vol. 36, no. 2, Article ID L02608, 5 pages, 2009.
- [15] S. Gleason and D. Gebre-Egziabher, "Remote sensing using bistatic GNSS reflections," in *GNSS Applications and Methods*, chapter 16, Artech House, 2009.
- [16] A. Awada, A. Khenchaf, and A. Coatanhay, "Frequency impact on the bistatic radar scattering from an ocean surface," in *Proceedings of the IEEE International Geoscience and Remote Sensing Symposium (IGARSS '07)*, pp. 4459–4462, Barcelona, Spain, June 2007.
- [17] J. Gower, "The 26 December 2004 tsunami measured by satellite altimetry," *International Journal of Remote Sensing*, vol. 28, no. 13-14, pp. 2897–2913, 2007.
- [18] C. Li, W. Huang, and S. Gleason, "Dual antenna space-based GNSS-R ocean surface mapping: oil slick and tropical cyclone sensing," *IEEE Journal of Selected Topics in Applied Earth Observations and Remote Sensing*, vol. 8, no. 1, pp. 425–435, 2015.
- [19] C. Ruf, M. Unwin, J. Dickinson et al., "CYGNSS: enabling the future of hurricane prediction [remote sensing satellites]," *IEEE Geoscience and Remote Sensing Magazine*, vol. 1, no. 2, pp. 52–67, 2013.



**Hindawi**

Submit your manuscripts at  
<http://www.hindawi.com>

